

On the Schrödingerization method for linear non-unitary dynamics with optimal dependence on matrix queries

Shi Jin^{*1}, Nana Liu^{† 1, 2}, Chuwen Ma^{‡1}, and Yue Yu^{§ ¶3}

¹School of Mathematical Sciences, Institute of Natural Sciences, MOE-LSC, Shanghai Jiao Tong University, Shanghai, 200240, China

²University of Michigan-Shanghai Jiao Tong University Joint Institute, Shanghai 200240, China

³Hunan Key Laboratory for Computation and Simulation in Science and Engineering, Key Laboratory of Intelligent Computing and Information Processing of Ministry of Education, National Center for Applied Mathematics in Hunan, School of Mathematics and Computational Science, Xiangtan University, Xiangtan, Hunan 411105, China

May 2, 2025

Abstract

The Schrödingerization method converts linear partial and ordinary differential equations with non-unitary dynamics into systems of Schrödinger-type equations with unitary evolution. It does so via the so-called warped phase transformation that maps the original equation into a Schrödinger-type equation in one higher dimension [1, 2]. We show that by employing a smooth initialization of the warped phase transform [3], Schrödingerization can in fact achieve optimal scaling in matrix queries. This paper presents the detailed implementation of three smooth initializations for the Schrödingerization method: (a) the cut-off function, (b) the higher-order polynomial interpolation, and (c) the Fourier transform methods, that achieve optimality for (a) and near-optimality for (b) and (c). A detailed analysis of key parameters affecting time complexity is conducted.

Contents

1 Introduction

^{*}shijin-m@sjtu.edu.cn

[†]nana.liu@quantumlah.org

[‡]chuwenii@sjtu.edu.cn

[§]terenceyuyue@xtu.edu.cn

[¶]Corresponding author.

2	The Schrödingerization method for non-unitary dynamics	4
2.1	The Schrödingerization method	5
2.2	Quantum simulation for time-dependent Schrödingerized system	6
2.3	Hamiltonian system for quantum computing	7
2.4	Detailed implementation of the Hamiltonian simulation	8
2.5	Complexity analysis	9
3	Optimal scaling in matrix queries with smooth initializations	10
4	Methods for smooth initializations	12
4.1	Cut-off function	12
4.2	Higher-order interpolation	14
4.3	Fourier transform	15
5	Discussions	15

1 Introduction

Quantum computing, an emerging technology, utilizes the principles of quantum mechanics to achieve unprecedented computational power [4–7]. Quantum algorithms operate within an n -qubit Hilbert space of dimension 2^n , potentially offering polynomial to even exponential computational advantage for models involving vast amounts of data. Hence, it has become an attractive computational paradigm to handle large-scale scientific computing problems that are bottlenecks for classical computation. A natural application is partial differential equations (PDEs) from time-dependent Schrödinger equations, which follow unitary evolutions and hence the wave functions can be coherently represented on quantum computers. Known as Hamiltonian simulations, a variety of efficient algorithms have been developed toward this goal [2, 8–17].

However, many physical phenomena – such as combustion, atmospheric and oceanic circulation, and electromagnetic wave propagation with physical boundaries – exhibit non-unitary dynamics. Even the time-dependent Schrödinger equation becomes non-unitary when artificial boundary conditions are introduced, making traditional Hamiltonian simulation techniques inapplicable [18]. Alternatively, crafting quantum PDE solvers involves discretising spatial variables to formulate a system of ordinary differential equations (ODEs), which can then be tackled using quantum ODE solvers [19–21]. Crucially, if the solution operator for the resulting ODE system is unitary, quantum simulations can achieve reduced time complexity compared to other quantum linear algebra methods like quantum difference methods [19, 22]. In cases where the system is not unitary – such as when incorporating physical boundary conditions – it becomes necessary to “dilate” it to a unitary system [2, 23–25].

Among the unitarization techniques, the *Schrödingerization* method proposed in [1, 2] offers a simple and general framework enabling quantum simulation for *all* linear PDEs and ODEs. It employs a warped phase transformation to lift the original equations into a higher-dimensional space, where they become Schrödinger-type equations – with unitary evolutions – in the Fourier

domain! This method has since been extended to a wide range of settings, including open quantum systems with non-unitary artificial boundary conditions [18], systems with physical boundary and interface conditions [26], Maxwell’s equations [27, 28], the Fokker-Planck equation [29], ill-posed problems such as the backward heat equation [3]. It has also been applied in iterative linear algebra solvers [30]. Moreover, as a naturally continuous-variable method [31], it represents the only viable approach so far for analog quantum simulation of PDEs and ODEs. The method can also be adapted to parabolic PDEs using a Jaynes-Cummings-type model, which is more readily available in current experiments [32].

In this article, we focus on the optimal scaling behavior of the Schrödingerization method for non-unitary dynamics. In the original Schrödingerization method, a simple even-function is used in the initial data in the extended variable, resulting only in a first-order approximation, which would require extra $\mathcal{O}(1/\varepsilon)$ qubits, where ε is the precision, if a qubit-based quantum algorithm is used. As already pointed out in [3], we can achieve improved – near optimal – scaling by employing a smoother initialization. We consider linear dynamical systems with a general evolution operator $A(t)$ and an inhomogeneous term $\mathbf{b}(t)$ as given in (2.1), and present a detailed implementation of the corresponding quantum algorithm using block-encoding techniques as described in [33, 34]. In our implementation, we first transform the system into a homogeneous one by enlarging the system with an auxiliary variable. Using the Schrödingerization method, we then transform it into a Hamiltonian system, which can be efficiently solved on quantum computers. For time-dependent Hamiltonian dynamics, we apply the quantum simulation technique from [25, 35] for non-autonomous systems. This technique involves transforming a non-autonomous system into an autonomous one in a higher dimension, avoiding the need for the complicated Dyson series. Consequently, we focus exclusively on analyzing the optimal dependence in the time-independent case. Through a detailed analysis of the parameters affecting time complexity, we find that the query complexity scales linearly with μ_{\max} , the maximum Fourier mode in absolute value, for the extended variable p with a generic initialization function $\psi(p)$ in the p -domain. Since μ_{\max} scales as $\mathcal{O}(1/\Delta p^r)$, where Δp is the mesh size in p , when $\psi(p) \in H^r$, we conclude that sufficiently smooth initializations can offer nearly exponential speedup in p variable over the original Schrödingerization method in terms of precision ε . Furthermore, for three types of smooth initializations: (a) cut-off functions, (b) higher-order interpolation, and (c) Fourier transform methods, we demonstrate that Schrödingerization achieves optimal matrix-query scaling with respect to the block-encoding oracle for (a) and near-optimality for (b) and (c).

In Table 1, we compare our algorithm with previous approaches in the homogeneous case. It is evident that the Schrödingerization method, with sufficiently smooth initialization in p , achieves both optimal state preparation cost and optimal dependence of the number of queries to the matrix on all parameters. We also note that the improvement in the LCHS method in [34] only leads to a sub-optimal dependence on matrix queries, as β cannot be exactly equal to 1 (i.e., $1/\beta > 1$), where β is the parameter in the kernel function of the improved LCHS.

The paper is structured as follows: In Section 2, we offer an overview of the Schrödingerization approach and present the full implementation by using block-encoding techniques. Section 3 demon-

Table 1: Comparison among improved Schrödingerization and previous methods for homogeneous dynamical systems. Here, $\alpha_A \geq \|A\|$, T is the evolution time, ε is the error, and $\beta \in (0, 1)$. All but the spectral method assume the real part of A to be positive semi-definite, while in the spectral method A is assumed to be diagonalizable with matrix V such that $\kappa_V \geq \|V^{-1}\| \|V\|$ and all the eigenvalues of A have non-negative real parts.

Method	Queries to A	Queries to \mathbf{u}_0
Spectral method [21]	$\tilde{\mathcal{O}}(\frac{\ \mathbf{u}_0\ }{\ \mathbf{u}(T)\ } \kappa_V \alpha_A T \text{poly}(\log \frac{1}{\varepsilon}))$	$\tilde{\mathcal{O}}(\frac{\ \mathbf{u}_0\ }{\ \mathbf{u}(T)\ } \kappa_V \alpha_A T \text{poly}(\log \frac{1}{\varepsilon}))$
Truncated Dyson [14]	$\tilde{\mathcal{O}}(\frac{\ \mathbf{u}_0\ }{\ \mathbf{u}(T)\ } \alpha_A T (\log \frac{1}{\varepsilon})^2)$	$\mathcal{O}(\frac{\ \mathbf{u}_0\ }{\ \mathbf{u}(T)\ } \alpha_A T \log \frac{1}{\varepsilon})$
Time-marching [17]	$\tilde{\mathcal{O}}(\frac{\ \mathbf{u}_0\ }{\ \mathbf{u}(T)\ } \alpha_A^2 T^2 \log \frac{1}{\varepsilon})$	$\mathcal{O}(\frac{\ \mathbf{u}_0\ }{\ \mathbf{u}(T)\ })$
Improved LCHS time-dependent [34]	$\tilde{\mathcal{O}}(\frac{\ \mathbf{u}_0\ }{\ \mathbf{u}(T)\ } \alpha_A T (\log \frac{1}{\varepsilon})^{1+1/\beta})$	$\mathcal{O}(\frac{\ \mathbf{u}_0\ }{\ \mathbf{u}(T)\ })$
Improved LCHS time-independent [34]	$\tilde{\mathcal{O}}(\frac{\ \mathbf{u}_0\ }{\ \mathbf{u}(T)\ } \alpha_A T (\log \frac{1}{\varepsilon})^{1/\beta})$	$\mathcal{O}(\frac{\ \mathbf{u}_0\ }{\ \mathbf{u}(T)\ })$
This work, time-dependent	$\tilde{\mathcal{O}}(\frac{\ \mathbf{u}_0\ }{\ \mathbf{u}(T)\ } \alpha_A T (\log \frac{1}{\varepsilon})^2)$	$\mathcal{O}(\frac{\ \mathbf{u}_0\ }{\ \mathbf{u}(T)\ })$
This work, time-independent	$\tilde{\mathcal{O}}(\frac{\ \mathbf{u}_0\ }{\ \mathbf{u}(T)\ } \alpha_A T \log \frac{1}{\varepsilon})$	$\mathcal{O}(\frac{\ \mathbf{u}_0\ }{\ \mathbf{u}(T)\ })$

strates how optimal scaling in matrix queries can be attained through the use of smooth initializations of the warped phase transformation. Section 4 outlines three approaches for constructing this smooth extension. Finally, some discussions are presented in the last section.

2 The Schrödingerization method for non-unitary dynamics

Consider a system of linear dynamical system in the form

$$\begin{cases} \frac{d}{dt} \mathbf{u}(t) = A(t) \mathbf{u}(t) + \mathbf{b}(t), & t \in (0, T), \\ \mathbf{u}(0) = \mathbf{u}_0, \end{cases} \quad (2.1)$$

where T is the evolution time, $\mathbf{u} = [u_0, u_1, \dots, u_{N-1}]^\top$, $\mathbf{b} = [b_0, b_1, \dots, b_{N-1}]^\top \in \mathbb{C}^N$ and $A \in \mathbb{C}^{N \times N}$. In general, A is not anti-Hermitian, i.e., $A^\dagger \neq -A$, where " \dagger " denotes conjugate transpose. When A is a linear operator, (2.1) is a system of ODEs. When A is a linear differential operator, (2.1) is a system of PDEs. By introducing an auxiliary vector function $\mathbf{r}(t)$ that remains constant in time if $\mathbf{b} \neq 0$, system (2.1) can be rewritten as a homogeneous system

$$\frac{d}{dt} \mathbf{u}_f = A_f \mathbf{u}_f, \quad A_f = \begin{bmatrix} A & B \\ O & O \end{bmatrix}, \quad \mathbf{u}_f(0) = \begin{bmatrix} \mathbf{u}_0 \\ \mathbf{r}_0 \end{bmatrix}, \quad (2.2)$$

where $B = \text{diag}\{b_0/\gamma_0, \dots, b_{N-1}/\gamma_{N-1}\}$ and $\mathbf{r}_0 = \text{diag}\{\gamma_0, \dots, \gamma_{N-1}\}$, with

$$\gamma_i = T \sup_{t \in [0, T]} |b_i(t)|, \quad i = 0, 1, \dots, N-1. \quad (2.3)$$

Here, each $\sup_{t \in [0, T]} |b_i(t)|$ can be replaced by its upper bound and we set $b_i/\gamma_i = 0$ if $b_i(t) \equiv 0$.

2.1 The Schrödingerization method

In this section, we briefly review the Schrödingerization approach for general linear dynamical systems. For a general A_f , we first decompose A_f into a Hermitian term and an anti-Hermitian term:

$$A_f(t) = H_1(t) + iH_2(t), \quad i = \sqrt{-1},$$

where

$$H_1(t) = \frac{A_f(t) + A_f^\dagger(t)}{2} = \begin{bmatrix} H_1^A & \frac{B}{2} \\ \frac{B^\top}{2} & O \end{bmatrix}, \quad H_2(t) = \frac{A_f(t) - A_f^\dagger(t)}{2i} = \begin{bmatrix} H_2^A & \frac{B}{2i} \\ -\frac{B^\top}{2i} & O \end{bmatrix},$$

with $H_1^A = (A + A^\dagger)/2$ and $H_2^A = (A - A^\dagger)/(2i)$. Throughout the article, we assume that the real part matrix H_1^A is negative semi-definite. More general cases are addressed in [3, 29, 36].

Using the warped phase transformation $\mathbf{w}(t, p) = e^{-p}\mathbf{u}_f(t)$ for $p \geq 0$ and symmetrically extending the initial data to $p < 0$, system (2.1) is then transformed to a system of linear convection equations [1, 2]:

$$\begin{cases} \frac{d}{dt}\mathbf{w}(t, p) = -H_1(t)\partial_p\mathbf{w} + iH_2(t)\mathbf{w}, \\ \mathbf{w}(0, p) = \psi(p)\mathbf{u}_0, \end{cases} \quad (2.4)$$

where $\psi(p) := e^{-|p|}$. According to [36, Theorem 3.1], we can restore the solution $\mathbf{u}_f(t)$ by

$$\mathbf{u}_f = e^p\mathbf{w}(t, p), \quad p \geq p^\diamond = \lambda_{\max}^+(H_1)T. \quad (2.5)$$

Here $\lambda_{\max}^+(H_1)$ is defined by

$$\lambda_{\max}^+(H_1) = \begin{cases} \sup_{\lambda \in \sigma(H_1(t)) \ 0 < t < T, 0 < \lambda} |\lambda|, & \text{if } \exists \lambda > 0 \text{ in } \sigma(H_1(t)) \text{ over } [0, T], \\ 0, & \text{otherwise,} \end{cases} \quad (2.6)$$

with $\sigma(H_1)$ the set of eigenvalues of H_1 . Since H_1^A is negative, it is easy to find from (2.3) that

$$\lambda_{\max}^+(H_1)T \leq \frac{1}{2}\|B\|_{\max}T \leq \frac{1}{2}.$$

For numerical implementation, we truncate the extended region to a finite interval $p \in [-L, R]$ with $L > 0$ and $R > 0$ satisfying

$$e^{-L+\lambda_{\max}^-(H_1)T} \approx e^{R-\lambda_{\max}^+(H_1)T} \approx 0. \quad (2.7)$$

The definition of $\lambda_{\max}^-(H_1)$ is similar to that in (2.6), denoting the largest absolute value among the negative eigenvalues of H_1 . Then one can apply the periodic boundary condition in the p direction and use the Fourier spectral method by discretising the p domain. Toward this end, we choose a uniform mesh size $\Delta p = (R + L)/N_p$ for the auxiliary variable with $N_p = 2^{n_p}$ being an even number, with the grid points denoted by $-L = p_0 < p_1 < \dots < p_{N_p} = R$. To compute $\mathbf{w}(t, p)$, let the vector \mathbf{w}_h be the collection of the function \mathbf{w} at these grid points, defined more precisely as $\mathbf{w}_h(t) = \sum_{k,i} \mathbf{w}_i(t, p_k)|k, i\rangle$, where \mathbf{w}_i is the i -th entry of \mathbf{w} .

By applying the discrete Fourier transform in the p direction, one arrives at

$$\frac{d}{dt}\mathbf{w}_h(t) = -i(P_\mu \otimes H_1)\mathbf{w}_h + i(I \otimes H_2)\mathbf{w}_h, \quad \mathbf{w}_h(0) = [\psi(p_0), \dots, \psi(p_{N_p-1})]^\top \otimes \mathbf{u}_0. \quad (2.8)$$

Here, P_μ is the matrix expression of the momentum operator $-i\partial_p$, given by

$$P_\mu = \Phi D_\mu \Phi^{-1}, \quad D_\mu = \text{diag}(\mu_0, \dots, \mu_{N_p-1}), \quad (2.9)$$

where $\mu_k = \frac{2\pi}{R+L}(k - \frac{N_p}{2})$ are the Fourier modes and

$$\Phi = (\phi_{jl})_{N_p \times N_p} = (\phi_l(x_j))_{N_p \times N_p}, \quad \phi_l(x) = e^{i\mu_l(x+L)}$$

is the matrix representation of the discrete Fourier transform. At this point, we have successfully mapped the dynamics back to a Hamiltonian system. By a change of variables $\tilde{\mathbf{w}}_h = (\Phi^{-1} \otimes I)\mathbf{w}_h$, one has

$$\frac{d}{dt}\tilde{\mathbf{w}}_h(t) = -iH(t)\tilde{\mathbf{w}}_h(t), \quad (2.10)$$

where $H = D_\mu \otimes H_1 - I \otimes H_2$.

2.2 Quantum simulation for time-dependent Schrödingerized system

If the coefficient in the dynamical system is time-dependent, namely a non-autonomous system, one can turn it into an autonomous unitary system via dimension lifting [25]. First, via Schrödingerization, one obtains a time-dependent Hamiltonian

$$\frac{d}{dt}\tilde{\mathbf{w}}_h = -iH(t)\tilde{\mathbf{w}}_h, \quad H = H^\dagger. \quad (2.11)$$

By introducing a new “time” variable s , the problem becomes a new linear PDE defined in one higher dimension but with time-independent coefficients,

$$\frac{\partial \mathbf{v}}{\partial t} = -\frac{\partial \mathbf{v}}{\partial s} - iH(s)\mathbf{v} \quad \mathbf{v}(0, s) = \delta(s)\tilde{\mathbf{w}}_h(0), \quad s \in \mathbb{R}, \quad (2.12)$$

where $\delta(s)$ is the dirac δ -function. One can easily recover $\tilde{\mathbf{w}}_h$ by $\tilde{\mathbf{w}}_h = \int_{-\infty}^{\infty} \mathbf{v}(t, s) ds$.

Since \mathbf{v} decays to zero as s approaches infinity, the s -region can be truncated to $[-\pi S, \pi S]$, where $\pi S > 4\omega + T$, with 2ω representing the length of the support set of the approximated delta function. Choosing S sufficiently large ensures that the compact support of the approximated delta function remains entirely within the computational domain throughout the simulation, allowing the spectral method to be applied. The transformation and difference matrix are defined by

$$(\Phi_s)_{lj} = (e^{i\mu_l^s(j\Delta s)}), \quad D_s = \text{diag}\{\mu_0^s, \mu_1^s, \dots, \mu_{N_s-1}^s\}, \quad \mu_l^s = (l - \frac{N_s}{2})S, \quad l, j \in [N_s],$$

where $\Delta s = 2\pi S/N_s$. Applying the discrete Fourier spectral discretization, it yields a time-independent Hamiltonian system as

$$\frac{d}{dt}\tilde{\mathbf{v}}_h = -i(D_s \otimes I + I_{N_s} \otimes H)\tilde{\mathbf{v}}_h, \quad \tilde{\mathbf{v}}_h(0) = [\Phi_s^{-1} \otimes I](\delta_h \otimes \tilde{\mathbf{w}}_h(0)), \quad (2.13)$$

where $\delta_h = \sum_{j \in [N_s]} \delta_\omega(s_j)|j\rangle$ with $s_j = -\pi S + j\Delta s$ and δ_ω is an approximation to δ function defined, for example, by choosing

$$\delta_\omega(x) = \frac{1}{\omega} \left(1 - \frac{1}{2} |1 + \cos(\pi \frac{x}{\omega})| \right) \quad |x| \leq \omega, \quad \delta_\omega(x) = 0 \quad |x| \geq \omega.$$

Here $\omega = m\Delta s$, where m is the number of mesh points within the support of δ_ω .

2.3 Hamiltonian system for quantum computing

As discussed in Section 2.2, a time-dependent system can be transformed into a time-independent system by adding an additional dimension. Therefore, the subsequent discussion will focus exclusively on the time-independent case. For further details on time-dependent systems, we refer to [35].

From (2.10), a quantum simulation can be carried out on the Hamiltonian system above:

$$|\mathbf{w}_h(T)\rangle = [\Phi \otimes I] \cdot \mathcal{U}(T) \cdot [\Phi^{-1} \otimes I] |\mathbf{w}_h(0)\rangle,$$

where $\mathcal{U}(T) = e^{-iHT}$ is a unitary operator, and Φ (or Φ^{-1}) is completed by (inverse) quantum Fourier transform (QFT or IQFT). The complete circuit for implementing the quantum simulation of $|\mathbf{w}_h\rangle$ is illustrated in Fig. 1.

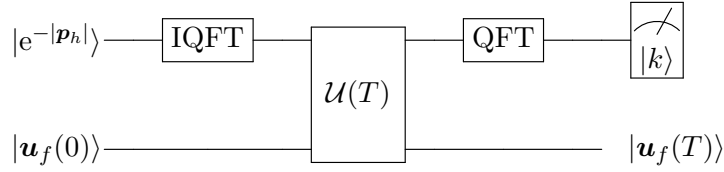


Fig. 1: Quantum circuit for Schrödingerization of (2.10).

From (2.5), one can recover the target variables for \mathbf{u}_f by performing a measurement in the computational basis:

$$M_k = |k\rangle\langle k| \otimes I, \quad k \in \{j : p_j \geq p^\diamond \text{ and } e^{p_j} = \mathcal{O}(1)\} =: I_\diamond,$$

where I_\diamond is referred to as the recovery index set. The state vector is then collapsed to

$$|\mathbf{w}_*\rangle \equiv |k_*\rangle \otimes \frac{1}{\mathcal{N}} \left(\sum_i w_{k_*i} |i\rangle \right), \quad \mathcal{N} = \left(\sum_i |w_{k_*i}|^2 \right)^{1/2}$$

for some k_* in the recover index set I_\diamond with the probability

$$P_r(t, p_{k_*}) = \frac{\sum_i |w_{k_*i}|^2}{\sum_{k,i} |w_{ki}(T)|^2} = \frac{\sum_i |\mathbf{w}_{i,h}(T, p_{k_*})|^2}{\sum_{k,i} |\mathbf{w}_{i,h}(T, p_k)|^2} = \frac{\|\mathbf{w}_h(T, p_{k_*})\|^2}{\sum_k \|\mathbf{w}_h(T, p_k)\|^2}.$$

Then the likelihood of acquiring $|\mathbf{w}_*\rangle$ that satisfies $k_* \in I_\diamond$ is given by

$$P_r^* = \frac{\sum_{k \in I_\diamond} \|\mathbf{w}_h(T, p_k)\|^2}{\sum_k \|\mathbf{w}_h(T, p_k)\|^2} = \frac{C_{e0}^2 \|\mathbf{u}_f(T)\|^2}{C_e^2 \|\mathbf{u}_f(0)\|^2},$$

where

$$C_{e0} = \left(\sum_{p_k \geq p^\diamond} (\psi(p_k))^2 \right)^{1/2}, \quad C_e = \left(\sum_{k=0}^{N_p-1} (\psi(p_k))^2 \right)^{1/2}, \quad \psi(p) = e^{-|p|}. \quad (2.14)$$

If N_p is sufficiently large, we have

$$\Delta p C_{e0}^2 \approx \int_{p^\diamond}^{\infty} e^{-2p} dp = \frac{1}{2} e^{-2p^\diamond}, \quad \Delta p C_e^2 \approx \int_{-\infty}^{\infty} e^{-2p} dp = 1,$$

where $\Delta p = (R + L)/N_p$, then it yields

$$\frac{C_{e0}^2}{C_e^2} \approx \frac{1}{2} e^{-2p^\diamond} = \frac{1}{2} e^{-1}. \quad (2.15)$$

Since $\mathbf{u}_f(t) = \begin{bmatrix} \mathbf{u}(t) \\ \mathbf{r}_0 \end{bmatrix}$, one can perform a projection to get $|\mathbf{u}(T)\rangle$ with the probability $\frac{\|\mathbf{u}(T)\|^2}{\|\mathbf{u}_f(T)\|^2}$.

The overall probability is then approximated by

$$P_u = \frac{C_{e0}^2 \|\mathbf{u}(T)\|^2}{C_e^2 \|\mathbf{u}_f(0)\|^2} = \frac{C_{e0}^2}{C_e^2} \frac{\|\mathbf{u}(T)\|^2}{\|\mathbf{u}_0\|^2 + T^2 \|\mathbf{b}\|_{\text{smax}}^2},$$

where

$$\|\mathbf{b}\|_{\text{smax}}^2 = \sum_{i=0}^{N-1} \left(\sup_{t \in [0, T]} |b_i(t)| \right)^2. \quad (2.16)$$

By using the amplitude amplification, the repeated times for the measurements can be approximated as

$$g = \mathcal{O}\left(\frac{C_e}{C_{e0}} \frac{\|\mathbf{u}_f(0)\|}{\|\mathbf{u}(T)\|}\right) = \mathcal{O}\left(\frac{\|\mathbf{u}_0\| + T\|\mathbf{b}\|_{\text{smax}}}{\|\mathbf{u}(T)\|}\right). \quad (2.17)$$

The quantity g in (2.17) is comparable to the number of repeated times by directly projecting onto $|k_*\rangle|0\rangle$ for $k_* \in I_\diamond$.

2.4 Detailed implementation of the Hamiltonian simulation

For the Hamiltonian simulation of $\mathcal{U}(T) = e^{-iHT}$, where H arises from the time-dependent system, one can apply established quantum algorithms from the literature. For instance, Hamiltonian simulation with nearly optimal dependence on all parameters is discussed in [9], where sparse access to the Hamiltonian H is assumed.

One can express the evolution operator $\mathcal{U}(T)$ as a select oracle

$$\mathcal{U}(T) = \sum_{k=0}^{N_p-1} |k\rangle\langle k| \otimes e^{-i(\mu_k H_1 - H_2)T} =: \sum_{k=0}^{N_p-1} |k\rangle\langle k| \otimes V_k(T).$$

Since the unitary $V_k(T)$ corresponds to the simulation of the Hamiltonian $H_{\mu_k} := \mu_k H_1 - H_2$, we assume the block-encoding oracles encoding the real and imaginary parts separately, namely

$$(\langle 0|_a \otimes I) U_{H_i} (|0\rangle_a \otimes I) = \frac{H_i}{\alpha_i}, \quad i = 1, 2,$$

where $\alpha_i \geq \|H_i\|$ is the block-encoding factor for $i = 1, 2$.

According to the discussion in [34, Section 4.2.1], there is an oracle HAM-T_{H_μ} such that

$$(\langle 0|_{a'} \otimes I) \text{HAM-T}_{H_\mu} (|0\rangle_{a'} \otimes I) = \sum_{k=0}^{N_p-1} |k\rangle\langle k| \otimes \frac{H_{\mu_k}}{\alpha_1 \mu_{\text{max}} + \alpha_2}, \quad (2.18)$$

where $H_{\mu_k} = \mu_k H_1 - H_2$ and $\mu_{\text{max}} = \max_k |\mu_k|$ represent the maximum absolute value among the discrete Fourier modes. This oracle only uses $\mathcal{O}(1)$ queries to block-encoding oracles for H_1 and H_2 . With the block-encoding oracle HAM-T_{H_μ} , we can implement

$$\text{SEL}_0 = \sum_{k=0}^{N_p-1} |k\rangle\langle k| \otimes V_k^a(T),$$

a block-encoding of $\mathcal{U}(T)$, using the quantum singular value transformation (QSVT) [37] for example, where $V_k^a(T)$ block-encodes $V_k(T)$ with $\|V_k^a(T) - V_k(T)\| \leq \delta$. This uses the oracles for H_1 and H_2

$$\mathcal{O}\left((\alpha_1 \mu_{\text{max}} + \alpha_2)T + \log(1/\delta)\right) = \mathcal{O}(\alpha_H \mu_{\text{max}} T + \log(1/\delta)) \quad (2.19)$$

times (see [34, Corollary 16]), where $\alpha_H \geq \alpha_i$, $i = 1, 2$.

Applying the block-encoding circuit to the initial input state $|0\rangle_{a'}|\tilde{\mathbf{w}}_0\rangle$ gives

$$\text{SEL}_0|0\rangle_{a'}|\tilde{\mathbf{w}}_0\rangle = |0\rangle_{a'}\mathcal{U}^a(T)|\tilde{\mathbf{w}}_0\rangle + |\perp\rangle,$$

where $\mathcal{U}^a(T)$ is the approximation of $\mathcal{U}(T)$ and $\tilde{\mathbf{w}}_0 = (\Phi^{-1} \otimes I)\mathbf{w}_h(0)$. This step only needs one query to the state preparation oracle $O_{\tilde{\mathbf{w}}}$ for $\tilde{\mathbf{w}}_0$.

According to the preceding discussions, we may conclude that there exists a unitary V_0 such that

$$|0^{n_a}\rangle|0^w\rangle \xrightarrow{V_0} \frac{1}{\eta_0}|0^{n_a}\rangle \otimes \tilde{\mathbf{w}}_h^a + |\perp\rangle,$$

where $\tilde{\mathbf{w}}_h^a$ is the approximate solution of $\tilde{\mathbf{w}}_h$, given by

$$\tilde{\mathbf{w}}_h^a = \mathcal{U}^a(T)\tilde{\mathbf{w}}_0 \quad \text{and} \quad \eta_0 = \|\tilde{\mathbf{w}}_0\| = \|\mathbf{w}_h(0)\| \leq C_e\|\mathbf{u}_f(0)\| \lesssim \Delta p \sqrt{\|\mathbf{u}_0\|^2 + T^2\|\mathbf{b}\|_{\text{max}}^2}.$$

2.5 Complexity analysis

In this section, we focus on the complexity analysis of the Schrödingerization. According to [36, Theorem 4.4], the error between $\mathbf{u}_h^d = e^{p_k}(\langle k| \otimes I)\mathbf{w}_h$ and \mathbf{u} consists of two parts: one arises from the truncation of the extended domain used for computation in (2.7), and the other results from the spectral discretization in p . Suppose L and R are large enough satisfying (2.7), and $\Delta p = \mathcal{O}(\mu_{\text{max}})$ is small. It follows that

$$\|\mathbf{u}_h(T) - \mathbf{u}(T)\| \leq \frac{\varepsilon}{2}\|\mathbf{u}(T)\|. \quad (2.20)$$

Theorem 2.1. *Assume L and R are large enough and $\Delta p = \mathcal{O}(\mu_{\text{max}})$ is small enough to satisfy (2.20). There exists a quantum algorithm that prepares an ε -approximation of the state $|\mathbf{u}(T)\rangle$ with $\Omega(1)$ success probability and a flag indicating success, using*

$$\tilde{\mathcal{O}}\left(\frac{\|\mathbf{u}(0)\| + T\|\mathbf{b}\|_{\text{max}}}{\|\mathbf{u}(T)\|}(\alpha_H T \mu_{\text{max}} + \log \frac{\mu_{\text{max}}(\|\mathbf{u}(0)\| + T\|\mathbf{b}\|_{\text{max}})}{\varepsilon\|\mathbf{u}(T)\|})\right)$$

queries to the HAM- T_{H_μ} oracle, where $\alpha_H \geq \|H_i\|$, $i = 1, 2$, and using

$$\mathcal{O}\left(\frac{\|\mathbf{u}(0)\| + T\|\mathbf{b}\|_{\text{max}}}{\|\mathbf{u}(T)\|}\right)$$

queries to the state preparation oracle for $\tilde{\mathbf{w}}_0$, where $\|\mathbf{b}\|_{\text{max}}$ is defined in (2.16).

Proof. Based on the Hamiltonian simulation, the state for \mathbf{w}^a/η_0 can be prepared with $\eta_0 = \|\mathbf{w}_h(0)\|$, yielding the approximation state vector $|\mathbf{u}^a(T)\rangle$ for the solution $|\mathbf{u}(T)\rangle$. The error between $|\mathbf{u}\rangle$ and $|\mathbf{u}^a(T)\rangle$ is obtained by

$$\| |\mathbf{u}(T)\rangle - |\mathbf{u}^a(T)\rangle \| \leq \| |\mathbf{u}(T)\rangle - |\mathbf{u}_*\rangle \| + \| |\mathbf{u}_*\rangle - |\mathbf{u}^a(T)\rangle \|,$$

where $\mathbf{u}_* = e^{p_{k_*}}(\langle k_*| \otimes I)\mathbf{w}_h$, $k_* \in I_\diamond$. From (2.20), one has

$$\| |\mathbf{u}(T)\rangle - |\mathbf{u}_*\rangle \| \leq \frac{2\|\mathbf{u}(T) - \mathbf{u}_*\|}{\|\mathbf{u}(T)\|} \leq \frac{\varepsilon}{2}.$$

By neglecting the error in the implementation of $\mathcal{U}(T)$, there holds

$$\| |\mathbf{u}_*\rangle - |\mathbf{u}^a(T)\rangle \| \leq \frac{2\|\mathbf{u}_* - \mathbf{u}^a\|}{\|\mathbf{u}_*\|} \leq \frac{2e^{p_{k*}}\|\mathbf{w}_h - \mathbf{w}^a\|}{\|\mathbf{u}_*\|}. \quad (2.21)$$

To ensure the overall error remains within ε , we require $\| |\mathbf{u}_*\rangle - |\mathbf{u}^a\rangle \| \leq \varepsilon/2$, yielding

$$\| |\mathbf{w}_h\rangle - |\mathbf{w}^a\rangle \| \leq \frac{2\|\mathbf{w}_h - \mathbf{w}^a\|}{\|\mathbf{w}_h\|} \leq \frac{\varepsilon e^{-p_{k*}}\|\mathbf{u}_*\|}{2\eta_0} := \delta. \quad (2.22)$$

According to (2.19), the assumption of mesh size and (2.22), the time cost to implement $\mathcal{U}(T)$ is

$$\tilde{\mathcal{O}} \left(T\alpha_H\mu_{\max} + \log \frac{1}{\delta} \right) = \tilde{\mathcal{O}} \left(T\alpha_H\mu_{\max} + \log \frac{\mu_{\max}\sqrt{\|\mathbf{u}(0)\|^2 + T^2\|\mathbf{b}\|^2}}{\varepsilon\|\mathbf{u}(T)\|} \right).$$

The proof is finished by multiplying the repeated times shown in (2.17). \square

Remark 2.1. When there is no inhomogeneous term, the introduction of auxiliary constant variables is unnecessary. In this case, the total query complexity for H_1 and H_2 is $\tilde{\mathcal{O}}(\frac{\|\mathbf{u}(0)\|}{\|\mathbf{u}(T)\|}\alpha_H T\mu_{\max})$. When the system is time-dependent, we employ the approach described in Section 2.2 to obtain a time-independent Hamiltonian system by introducing an additional dimension. Following the analysis in Theorem 2.1, it is straightforward to derive that the query complexity for the time-dependent system is $\tilde{\mathcal{O}}(\frac{\|\mathbf{u}(0)\|}{\|\mathbf{u}(T)\|}\alpha_H T\mu_{\max}\mu_{\max}^s)$, where $\mu_{\max}^s = \max_{l \in [N_s]} |\mu_l^s|$.

Remark 2.2. Our method for solving (2.1) with a time-dependent source term encodes $\mathbf{b}(t)$ directly within the coefficient matrix. This results in the same query complexity for both the coefficient matrix $A(t)$ and $\mathbf{b}(t)$. To minimize the repeated use of the state preparation oracle O_b for the source term \mathbf{b} , when $\mathbf{b}(t)$ is time-independent, we can instead consider a simpler enlarged system

$$\frac{d}{dt}\mathbf{u}_f(t) = \begin{bmatrix} A & \frac{I}{T} \\ O & O \end{bmatrix} \mathbf{u}_f(t), \quad \mathbf{u}_f(t) = \begin{bmatrix} \mathbf{u}(t) \\ T\mathbf{b} \end{bmatrix}, \quad \mathbf{u}_f(0) = \begin{bmatrix} \mathbf{u}(0) \\ T\mathbf{b} \end{bmatrix}.$$

In the time-dependent case, it may be advantageous to separately implement their homogeneous and inhomogeneous parts and combine them using the LCU technique [34]. Each execution of the LCU procedure requires $\mathcal{O}(1)$ uses of the associated preparation oracles, with the overall complexity primarily dependent on the success probability.

3 Optimal scaling in matrix queries with smooth initializations

In this section, we demonstrate that the smooth extension to $p < 0$ for e^{-p} is sufficient to achieve optimal dependence on matrix queries.

The original Schrödingerization method exhibits first-order convergence in p due to the lack of regularity of $\psi(p) = e^{-|p|}$ in the initial data in (2.4). Consequently, achieving precision ε may require a large number $N_p = \mathcal{O}(1/\varepsilon)$. This results in the maximum absolute value among the discrete Fourier modes scaling as $\mathcal{O}(1/\varepsilon)$, i.e., $\mu_{\max} = \mathcal{O}(1/\varepsilon)$, which is not optimal because the query complexity may linearly depend on μ_{\max} as shown in Theorem 2.1.

Let $\psi(p) \in H^r((-L, R))$ and denote by $P_h\psi$ its approximation using the discrete Fourier transform. The standard error estimate gives

$$\|\psi - P_h\psi\| \lesssim \left(\frac{R+L}{N_p}\right)^r |\psi|_r.$$

It is important to note that this estimate applies not only to the initial data but also to the solution of (2.4), since \mathbf{w} satisfies a transport equation in the p direction thus preserves the regularity in p in the initial data as time evolves. Assuming the right-hand side equals ε , we find

$$N_p \sim (R+L)|\psi|_r^{1/r} \varepsilon^{-1/r}.$$

By requiring $(1/\varepsilon)^{1/r} \sim \log(1/\varepsilon)$, one has

$$N_p \sim (R+L)|\psi|_r^{1/r} \log(1/\varepsilon) \quad \text{if} \quad r \sim \frac{\log(1/\varepsilon)}{\log(\log(1/\varepsilon))}. \quad (3.1)$$

This suggests that choosing $\psi \in H^r((-L, R))$ with r logarithmic in terms of $1/\varepsilon$, and ensuring $|\psi|_k^{1/k} \leq C$ is uniformly bounded for $k \leq r$, is sufficient.

The specified regularity of $\psi(p)$ leads to

$$\mu_{\max} = \frac{N_p \pi}{R+L} = |\psi|_r^{1/r} \log(1/\varepsilon) = \mathcal{O}(\log(1/\varepsilon)). \quad (3.2)$$

Substituting this into Theorem 2.1, we conclude that the non-unitary dynamic system (2.1) can be simulated from $t = 0$ to $t = T$ with an error of ε , achieving $\tilde{\mathcal{O}}(\alpha_H T \log(1/\varepsilon))$ queries to the HAM- H_μ oracle. This demonstrates optimal dependence on matrix queries.

In summary of the preceding discussion, we can conclude that

Theorem 3.1. *Suppose that the inhomogeneous dynamical system in (2.1) is autonomous. Under the conditions of Theorem 2.1, assume that $\psi(p)$ in (2.4) is sufficiently smooth. Then there is a quantum algorithm that prepares an ε -approximation of the normalized solution $|\mathbf{u}(T)\rangle$ with $\Omega(1)$ probability and a flag indicating success, using*

$$\tilde{\mathcal{O}}\left(\frac{\|\mathbf{u}(0)\| + T\|\mathbf{b}\|_{\max}}{\|\mathbf{u}(T)\|} \alpha_H T \log(1/\varepsilon)\right)$$

queries to the HAM- T oracle in (2.18) and

$$\mathcal{O}\left(\frac{\|\mathbf{u}(0)\| + T\|\mathbf{b}\|_{\max}}{\|\mathbf{u}(T)\|}\right)$$

queries to the state preparation oracle for $[\psi(p_0), \dots, \psi(p_{N_p-1})]^\top \otimes \mathbf{u}_0$, where $\|\mathbf{b}\|_{\max}$ is defined in (2.16).

Remark 3.1. From Remark 2.1, we can deduce that for time-dependent systems, after applying the same smoothing technique, the query complexity approaches $\tilde{\mathcal{O}}(\frac{\|\mathbf{u}(0)\| + T\|\mathbf{b}\|_{\max}}{\|\mathbf{u}(T)\|} \alpha_H T (\log \frac{1}{\varepsilon})^2)$, which includes an additional logarithmic term with respect to ε , consistent with the observation in [34] (see Table 1 there).

4 Methods for smooth initializations

From (2.4), it is easy to find that the limitation of the convergence order mainly comes from the low regularity of $\psi(p) = e^{-|p|}$, which is continuous but not in $C^1(\mathbb{R})$. According to Section 3, in order to obtain the optimal scaling in matrix queries, we need to use sufficiently smooth initial data in the extended domain in p . In this section, we present three methods for constructing such a smooth extension.

4.1 Cut-off function

The cut-off function, which restricts the values of a function below a specified threshold, is a fundamental tool in the analysis of partial differential equations. In this subsection, we utilize the cut-off technique to construct the desired smooth extension.

We begin by recalling the mollifier, defined as

$$\eta(x) = \begin{cases} \frac{1}{C} \exp\left(\frac{1}{|x|^2-1}\right), & |x| < 1, \\ 0, & |x| \geq 1, \end{cases} \quad (4.1)$$

where B_1 denotes the unit ball in \mathbb{R}^n and C is the normalization constant ensuring $\int_{\mathbb{R}^n} \eta(x) dx = 1$. This function belongs to $C_0^\infty(\mathbb{R}^n)$ with support $\overline{B_1}$. For any $\varepsilon > 0$, we can rescale the function such that its support becomes $\overline{B_\varepsilon}$, a closed ball of radius ε . The rescaled function is given by $\eta_\varepsilon(x) = \frac{1}{\varepsilon^n} \eta\left(\frac{x}{\varepsilon}\right)$. For a function $u \in L_{\text{loc}}^1(\Omega)$, the mollifier operator J_ε is defined through convolution as

$$J_\varepsilon u(x) = (\eta_\varepsilon * u)(x) = \int_{\Omega} \eta_\varepsilon(x-y)u(y)dy = \int_{B_\varepsilon(x)} \eta_\varepsilon(x-y)u(y)dy, \quad x \in \Omega_\varepsilon,$$

where the domain Ω_ε is defined by

$$\Omega_\varepsilon = \left\{x \in \Omega : \overline{B_\varepsilon(x)} \subset \Omega\right\} = \{x \in \Omega : \text{dist}(x, \partial\Omega) > \varepsilon\}.$$

It can be verified that $J_\varepsilon u \in C^\infty(\Omega_\varepsilon)$ for every $u \in L_{\text{loc}}^1(\Omega)$. Furthermore, if $\text{supp}\{u\} \Subset \Omega$, denoting $\delta = \text{dist}(\text{supp}\{u\}, \partial\Omega)$, then for $\varepsilon < \delta/4$, we have $J_\varepsilon u \in C_0^\infty(\Omega)$ with $\text{supp}\{J_\varepsilon u\} \subset \Omega_\varepsilon$.

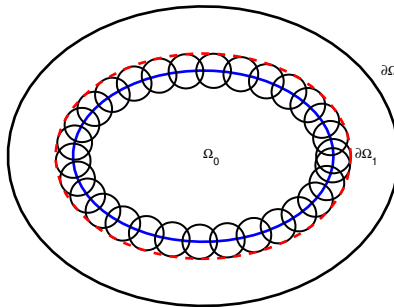


Fig. 2: A snapshot of the domain of the cut-off function in \mathbb{R}^2

Now we are ready to describe the construction of the cut-off function with the domain illustrated in Fig. 2.

Lemma 4.1 (cut-off function). *Let $\Omega \subset \mathbb{R}^n$ be a non-empty open set, and $\Omega_0 \Subset \Omega$. Define*

$$\delta = \text{dist}(\Omega_0, \partial\Omega), \quad d = \frac{\delta}{4}, \quad \Omega_1 = \{x \in \Omega : \text{dist}(x, \Omega_0) < d\}.$$

Let $\phi(x) = \chi_{\Omega_1}(x)$ denote the indicator function of Ω_1 . Then $\zeta = J_d\phi$ satisfies

$$\begin{cases} \zeta \in C_0^\infty(\Omega), & \text{supp}\{\zeta\} \subset K_d, \\ \zeta(x) \equiv 1, & x \in \Omega_0, \\ 0 \leq \zeta(x) \leq 1, & x \in \Omega, \end{cases}$$

where

$$K_d = \{x \in \Omega : \text{dist}(x, \Omega_1) \leq d\} = \{x \in \Omega : \text{dist}(x, \Omega_0) \leq 2d\}.$$

The function ζ is referred to as the cut-off function relative to the subset Ω_0 in Ω .

The cut-off function satisfies the following estimate for its derivatives:

$$|D^\alpha \zeta| \leq \frac{C}{d^{|\alpha|}},$$

where α is a multi-index and C is independent of $d = \delta/4$. This property is particularly advantageous for our extension.

For the Schrödingerization method, we set $\Omega_0 = (-1, R)$ and $d = 1$. Let $\psi(p) = \zeta(p)e^{-p}$. Then it holds that $\text{supp}\{\psi\} \subset [-3, R+2]$ and the derivatives of ψ are uniformly bounded. The cut-off function and the resulting smooth extension are shown in Fig. 3 for $R = 5$.

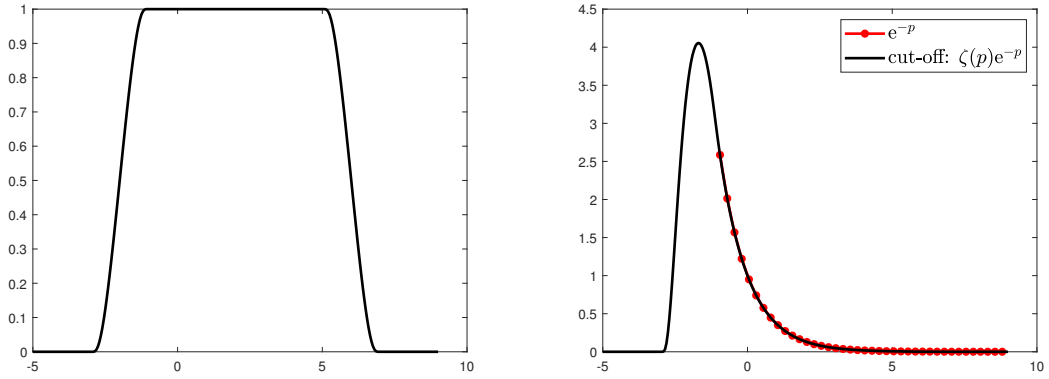


Fig. 3: The cut-off function and the resulting smooth extension

In the implementation, the computational domain for p can be selected as $[-L, R+2]$. It's important to note that the periodic boundary conditions can be satisfied for sufficiently small R when the real part matrix H_1 is negative semi-definite. This is because we only require $\|\psi\|_r^{1/r}$ to be bounded, not the H^r norm itself. In fact, we have $\|\psi\|_r^{1/r} \lesssim 1/d = \mathcal{O}(1)$ for any $r > 1$, leading to $\mu_{\max} = \mathcal{O}(\log(1/\varepsilon))$. Therefore, we obtain the optimal complexity by combining (3.2) and Theorem 2.1. In addition, the support of $\psi(p)$ can indeed be confined to a limited interval independent of the error tolerance. However, in cases where the real part matrix H_1 is not negative semi-definite, for the sake of a high probability of measurement, R should be sufficiently large such that $e^{-R} \approx 0$. In such scenarios, the computational domain may alternatively be chosen as $[-L, R]$.

4.2 Higher-order interpolation

An alternative approach to constructing the smooth function in the extended domain is to utilize high-order interpolations. To do so, we rewrite the initial function as

$$\psi(p) = \begin{cases} h(p), & p \in (-\infty, 0], \\ e^{-p}, & p \in (0, \infty), \end{cases}$$

where $h(p)$ is defined by

$$h(p) = \mathcal{P}_{2r-1}(p), \quad p \in [-1, 0], \quad h(p) = e^p, \quad p \in (-\infty, -1). \quad (4.2)$$

Here, $\mathcal{P}_{2r-1}(p)$ is a Hermite interpolation polynomial whose degree does not exceed $(2r-1)$ [38, Section 2.1.5], satisfying

$$\begin{aligned} (\partial_{p^k} \mathcal{P}_{2r-1}(p))|_{p=0} &= (\partial_{p^k} (e^{-p}))|_{p=0} = (-1)^k, \\ (\partial_{p^k} \mathcal{P}_{2r-1}(p))|_{p=-1} &= (\partial_{p^k} (e^p))|_{p=-1} = e^{-1}, \end{aligned}$$

where $0 \leq k \leq r-1$ is an integer. It is simple to check that $\psi \in C^{r-1}(\mathbb{R})$ and $\psi(p) \in H^r((-L, R))$ after restricting the extended domain to a limited interval. The explicit formula of $\mathcal{P}_{2r-1}(p)$ is given by

$$\mathcal{P}_{2r-1}(p) = \sum_{k=0}^{r-1} (e^{-1} L_{0k}(p) + (-1)^k L_{1k}(p)),$$

where L_{ik} are generalized Lagrange polynomials defined recursively for $k = r-2, r-3, \dots, 0$,

$$L_{0k}(p) := l_{0k}(p) - \sum_{\nu=k+1}^{r-1} l_{0k}^{(\nu)}(-1) L_{0\nu}(p), \quad L_{1k}(p) := l_{1k}(p) - \sum_{\nu=k+1}^{r-1} l_{1k}^{(\nu)}(0) L_{1\nu}(p),$$

with the starting polynomial for $k = r-1$

$$L_{0r-1}(p) := l_{0r-1}(p), \quad L_{1r-1}(p) := l_{1r-1}(p).$$

The auxiliary polynomials are

$$l_{0k}(p) := \frac{(-1)^r (p+1)^k p^r}{k!}, \quad l_{1k}(p) := \frac{p^k (p+1)^r}{k!}.$$

According to the discussion in [3], the target variable $\mathbf{u}(t) = e^p \mathbf{v}(t, p)$ still holds for all $p > 0$, since we do not care the solution when $p < 0$. We provide the snapshots of ψ for $r = 2, 4, 6, 8, 10$ in Fig. 4.

By employing the mollifier technique described in Section 4.1, we can identify a smooth function $\varphi \in C^\infty(\mathbb{R})$ such that $\varphi(p)|_{(-\infty, -1) \cup (0, \infty)} = e^{-|p|}$. Consequently, $\mathcal{P}_{2r-1}(p)$ can be interpreted as an interpolation of φ . Given that $\|\varphi^{(r)}\|_{L^\infty(-1, 0)}$ is bounded, the H^r norm of ψ over the finite interval $[-L, R]$ remains uniformly bounded. Unfortunately, while ψ is contained in H^r with any fixed $r \geq 1$, its exclusion from the C^∞ -class necessarily restricts the achievable complexity to a quasi-optimal order. For the Schrödingerization method, the truncation of the extended domain must satisfy (2.7), it follows that $\mathbf{w}(t, -L) \approx \mathbf{w}(t, R) \approx 0$ [36]. Therefore, spectral methods can be used.

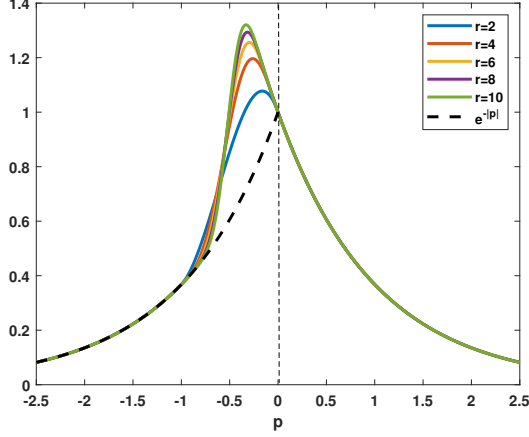


Fig. 4: The smooth initial data of $\psi(p)$ by using high-order interpolation.

4.3 Fourier transform

Building upon similar principles and utilizing the continuous Fourier transform in p , [39] introduces an algorithm for implementing Linear Combination of Hamiltonian Simulation (LCHS). The original LCHS approach in [39] is also a first-order method due to the slow decay rate of the integrand as a function of k , where k is the continuous Fourier mode. In the continuous scenario, the integrand function with respect to k is the Fourier transform of $\psi(p) = e^{-|p|}$, given by $\frac{1}{\pi(1+k^2)}$. It decays only quadratically, necessitating the truncation interval choice of $[-K, K]$ with $K = \log(1/\varepsilon)$. This introduces a computational overhead of $\mathcal{O}(1/\varepsilon)$, as $kH_1(s) - H_2(s)$ may have a spectral norm as large as $K\|H_1(s)\|$. This limitation was addressed in [34] by replacing the original integrand with a new kernel function decaying at a near-exponential rate $e^{-c|k|^\beta}$, where $\beta \in (0, 1)$. Consequently, they no longer need to truncate the interval at $K = \mathcal{O}(1/\varepsilon)$, and instead use the much smaller cutoff $K = (\log(1/\varepsilon))^{1/\beta}$. The improved LCHS method requires

$$\tilde{\mathcal{O}} \left(\frac{\|\mathbf{u}(0)\| + \|\mathbf{b}\|_{L^1}}{\|\mathbf{u}(T)\|} \alpha_H T (\log(1/\varepsilon))^\gamma \right)$$

queries to the HAM-T oracle, where $\gamma = 1 + 1/\beta$ and β for linear systems with time-dependent and time-independent coefficients, respectively. This leads to an exponential reduction in the Hamiltonian simulation time with respect to ε compared to the original LCHS. Since $\beta \in (0, 1)$, it holds that $1/\beta > 1$, indicating sub-optimal behavior with respect to queries to the HAM-T oracle.

We emphasize that the fundamental principle remains consistent with our approach with smooth initialization. Indeed, as illustrated in Fig. 5, the Fourier transforms of their kernel functions are e^{-x} for $x > 0$, whereas they exhibit significant differences on the negative real axis. Therefore, the transformed kernel function can be interpreted as a smooth extension in the p space.

5 Discussions

The LCHS in [39] utilizes the continuous Fourier transform in p and is a first-order method in the original version. Subsequent improvements in [34] refine the accuracy dependency of the

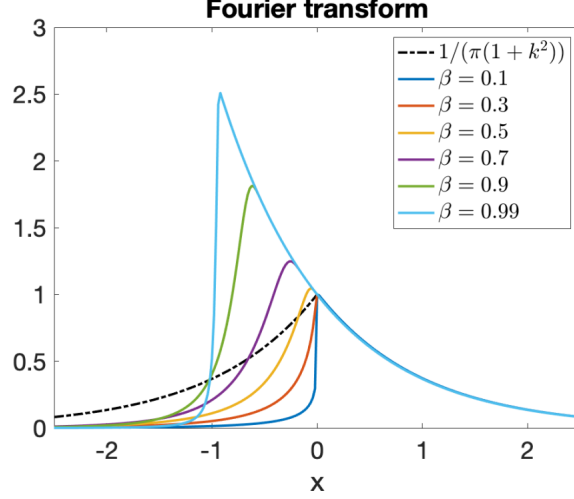


Fig. 5: Fourier transforms of the kernel functions (see Figure 3 of [34])

original LCHS algorithms by incorporating new kernel functions with faster decay and truncating the Fourier transform integral to a finite interval $[-K, K]$, where $K = (\log(1/\varepsilon))^{1/\beta}$ ($0 < \beta < 1$) truncates the continuous Fourier variable k . This approach results in sub-optimal dependence on matrix queries, $(\log(1/\varepsilon))^{1+1/\beta}$ for the time-dependent case, since β cannot be exactly equal to 1 (i.e., $1/\beta > 1$).

The smooth extension based on the Fourier transform is an adaptation of the kernel function method in [34]. Therefore, the method in [34] can be successfully integrated into our framework, as the transformed kernel function can be interpreted as a smooth extension in physical space.

Acknowledgements

SJ and NL are supported by NSFC grant No. 12341104, the Shanghai Jiao Tong University 2030 Initiative and the Fundamental Research Funds for the Central Universities. SJ was also partially supported by the Shanghai Municipal Science and Technology Major Project (2021SHZDZX0102). NL also acknowledges funding from NSFC grant No.12471411 and the Science and Technology Program of Shanghai, China (21JC1402900). CM was partially supported by the China Postdoctoral Science Foundation (No. 2023M732248) and the Postdoctoral Innovative Talents Support Program (No. BX20230219). YY was supported by NSFC grant No. 12301561, the Key Project of Scientific Research Project of Hunan Provincial Department of Education (No. 24A0100) and the 111 Project (No. D23017).

References

- [1] S. Jin, N. Liu, and Y. Yu. Quantum simulation of partial differential equations via Schrödingerization. *Phys. Rev. Lett.*, 133(23):230602, 2024.
- [2] S. Jin, N. Liu, and Y. Yu. Quantum simulation of partial differential equations: Applications and detailed analysis. *Phys. Rev. A*, 108:032603, 2023.

- [3] S. Jin, N. Liu, and C. Ma. Schrödingerisation based computationally stable algorithms for ill-posed problems in partial differential equations. *arXiv:2403.19123*, 2024.
- [4] J. D. Hidary. *Quantum Computing: An Applied Approach*. Springer, 2019.
- [5] M. A. Nielsen and I. L. Chuang. *Quantum Computation and Quantum Information*. Cambridge, New York, 2010.
- [6] J. Preskill. Quantum computing in the NISQ era and beyond. *Quantum*, 2:79, 2018.
- [7] E. G. Rieffel and W. H. Polak. *Quantum Computing: A Gentle Introduction*. MIT Press, 2011.
- [8] D. W. Berry, A. M. Childs, R. Cleve, R. Kothari, and R. D. Somma. Simulating Hamiltonian Dynamics with a truncated Taylor series. *Phys. Rev. Lett.*, 114(9), 2015.
- [9] D. W. Berry, A. M. Childs, and R. Kothari. Hamiltonian simulation with nearly optimal dependence on all parameters. In *2015 IEEE 56th Annual Symposium on Foundations of Computer Science*, pages 792–809, 2015.
- [10] D. W. Berry, A. M. Childs, R. Cleve, R. Kothari, and R. D. Somma. Exponential improvement in precision for simulating sparse Hamiltonians. *Forum of Mathematics, Sigma*, 5, 2017.
- [11] G. H Low and I. L. Chuang. Optimal Hamiltonian simulation by quantum signal processing. *Phys. Rev. Lett.*, 118(1), 2017.
- [12] G. H. Low and I. L. Chuang. Hamiltonian simulation by qubitization. *Quantum*, 3:163, 2019.
- [13] S. Chakraborty, A. Gilyén, and S. Jeffery. The power of block-encoded matrix powers: Improved regression techniques via faster Hamiltonian simulation. In *Proceedings of the 46th International Colloquium on Automata, Languages, and Programming (ICALP 2019)*, 2019.
- [14] M. Kieferová, A. Scherer, and D. W. Berry. Simulating the dynamics of time-dependent Hamiltonians with a truncated Dyson series. *Phys. Rev. A*, 99:042314, 13 pp., 2019.
- [15] D. An, D. Fang, and L. Lin. Time-dependent unbounded Hamiltonian simulation with vector norm scaling. *Quantum*, 5:459, 2021.
- [16] D. An, D. Fang, and L. Lin. Time-dependent Hamiltonian simulation of highly oscillatory dynamics and superconvergence for Schrödinger equation. *Quantum*, 6:690, 2022.
- [17] D. Fang, L. Lin, and Y. Tong. Time-marching based quantum solvers for time-dependent linear differential equations. *Quantum*, 7:955, 2023.
- [18] S. Jin, X. Li, N. Liu, and Y. Yu. Quantum simulation for quantum dynamics with artificial boundary conditions. *SIAM J. Sci. Comput.*, 46:B403–B421, 2024.
- [19] D. W. Berry. High-order quantum algorithm for solving linear differential equations. *J. Phys. A: Math. Theor.*, 47(10):105301, 17 pp., 2014.

- [20] D. W. Berry, A. M. Childs, A. Ostrander, and G. Wang. Quantum algorithm for linear differential equations with exponentially improved dependence on precision. *Comm. Math. Phys.*, 356(3):1057–1081, 2017.
- [21] A. W. Childs and J. Liu. Quantum spectral methods for differential equations. *Comm. Math. Phys.*, 375(2):1427–1457, 2020.
- [22] S. Jin, N. Liu, and Y. Yu. Time complexity analysis of quantum difference methods for linear high dimensional and multiscale partial differential equations. *J. Comput. Phys.*, 471:111641, 2022.
- [23] G. C. Javier, R. R. Angel, S. Enrique, and S. Mikel. Simulating option price dynamics with exponential quantum speedup. *arXiv:2101.04023v3*, 2022.
- [24] D. Burgarth, P. Facchi, and R. Hillier. Control of quantum noise: On the role of dilations. *Ann. Henri Poincaré*, 24:325–347, 2023.
- [25] Y. Cao, S. Jin, and N. Liu. Quantum simulation for time-dependent Hamiltonians – with applications to non-autonomous ordinary and partial differential equations. *arXiv:2312.02817*, 2023.
- [26] S. Jin, X. Li, N. Liu, and Y. Yu. Quantum simulation for partial differential equations with physical boundary or interface conditions. *J. Comp. Phys.*, 498:112707, 2024.
- [27] S. Jin, N. Liu, and C. Ma. Quantum simulation of Maxwell’s equations via Schrödingersation. *ESAIM, Math. Model. Numer. Anal.*, 58:1853–1879, 2024.
- [28] C. Ma, S. Jin, N. Liu, K. Wang, and L. Zhang. Schrödingerization based quantum circuits for Maxwell’s equation with time-dependent source terms. *arXiv:2411.10999*, 2024.
- [29] S. Jin, N. Liu, and Y. Yu. Quantum simulation of the Fokker-Planck equation via Schrödingerization. *arXiv:2404.13585v2*, 2024.
- [30] S. Jin and N. Liu. Quantum simulation of discrete linear dynamical systems and simple iterative methods in linear algebra via Schrödingerisation. *Proc. Royal Soc. London A*, page 20230370, 2024.
- [31] S. Jin and N. Liu. Analog quantum simulation of partial differential equations. *Quantum Sci. Technol.*, 2023.
- [32] S. Jin and N. Liu. Analog quantum simulation of parabolic partial differential equations using Jaynes-Cummings-like models. *arXiv:2407.01913*, 2024.
- [33] G. H. Low and N. Wiebe. Hamiltonian simulation in the interaction picture. *arXiv:1805.00675v2*, 2019.
- [34] D. An, A. W. Childs, and L. Lin. Quantum algorithm for linear non-unitary dynamics with near-optimal dependence on all parameters. *arXiv:2312.03916*, 2023.

- [35] Y. Cao, S. Jin, and N. Liu. A unifying framework for quantum simulation algorithms for time-dependent Hamiltonian dynamics. *arXiv:2411.03180*, 2024.
- [36] S. Jin, N. Liu, and C. Ma. On Schrödingerization based quantum algorithms for linear dynamical systems with inhomogeneous terms. *arXiv:2402.14696*, 2024.
- [37] A. Gilyén, Y. Su, G. H. Low, and N. Wiebe. Quantum singular value transformation and beyond: exponential improvements for quantum matrix arithmetics. In *Proceedings of the 51st Annual ACM SIGACT Symposium on Theory of Computing*, pages 193–204, 2019.
- [38] J. Stoer, R. Bulirsch, R. Bartels, W. Gautschi, and C. Witzgall. *Introduction to numerical analysis*. New York: Springer, 1980.
- [39] D. An, J. Liu, and L. Lin. Linear combination of Hamiltonian simulation for non-unitary dynamics with optimal state preparation cost. *Phys. Rev. Lett.*, 131(15):150603, 2023.